Beam Based Time Reversal Focused Imaging

T. Heilpern[1], *A. Shlivinski*[2], *E. Heyman*[3]

[1] School of Electrical Engineering, Tel Aviv University, Tel Aviv 69978, Israel. talhe@eng.tau.ac.il

[2] Department of Electrical and Computer Engineering, Ben-Gurion University of the Negev, Beer-Sheva 84105, Israel, amirshli@ee.bgu.ac.il

[3] School of Electrical Engineering, Tel Aviv University, Tel Aviv 69978, Israel. heyman@eng.tau.ac.il

Abstract

We present a beam-based time reversal imaging of point scatterers, using collimated iso-diffracting Gaussian beams for frequency domain applications, or pulsed beams for time domain applications. The formulation involves a beam-based data matrix relating the beam-transducers used as transmitters and receivers, but such matrix may also be synthesized in the preprocessing phase by a linear transformation of the data matrix corresponding to any other type of transducers. The beam-based data matrix is then used to create sparse time reversal operators for each sub-domain in the target domain.

1. Introduction

Time reversal (TR) imaging (also termed phase conjugation in frequency domain formulations) is commonly expressed in terms of the TR matrix which is calculated from the so called "data matrix" that records the signal in each receiver due to each of the (independent) sources. In the processing phase, the eigen-vectors of the TR marix are used to construct the image via either (a) *selective focusing* algorithms, where the eigen-vectors, when used as excitations to the source array, generate fields that focus on the point scatterers [1], or (b) the *multiple signal classification (MUSIC)* algorithm, where the point scatterers are shown to correspond to the poles of pseudo spectrum [2].

The TR imaging typically involves discrete wide angle (point-source like) transducers as sources and receivers. Here we present a self-consistent beam-based TR imaging formulations using collimated iso-diffracting Gaussian beams (ID-GB) for ultra wideband frequency domain (UWB-FD) applications, or pulsed beams (PB) for time domain (TD) applications. The beam formulations may consists of beam-transducers (e.g., wide aperture antennas or arrays of coherent antennas), in which case the data matrix records the signal in each beam receivers due to each beam-source excitation. However, one may also use any other set of transducers and then calculate the beam-based data matrix in the preprocessing phase by a proper linear transformation of the physical transducer data matrix. The beam basis provides a complete spectral representation of any source field, as an alternative to the conventional plane-wave or Green's function representations [3], but it has certain advantages that may be utilized in order to formulate efficient imaging and inverse scattering algorithms. The main advantage is the selective excitation of sub-domains in the target domain which localizes the imaging calculation and thus reduces the rank of the data-space associated with a given sub-domain. This also reduces the effect of irrelevant scattering contributions from targets that are outside the sub-domain of interest. Finally, beam-based schemes allow smooth extension to inhomogeneous medium which is insensitive to ray catastrophes (such as caustics).

Beam summation formulations have been used extensively in wave theory as a framework for ray-based construction of spectrally uniform solutions in complex configurations. In these formulations, the source-field is expanded into a spectrum of collimated beam propagators that emanate from the source in all directions, and thereafter are tracked locally in the medium and summed up at the observation points. Their main advantages are the spectral localization and the uniformity due to the fact that beam fields are insensitive to ray transition region (see [4, 5] and a recent review in [3]). Edelmann et al. [6] used phased array of point sources to generate beam-based TR imaging, yet the fields generated by such arrays are not standard beams, like GB's, and therefore cannot be tracked analytically in complex media. Beam based inversion were also studied in [7, 8, 9].

In this work the data is collected and organized in a beam to beam data matrix. The eigenvectors of this matrix can be used for imaging via field focusing or for creating the MUSIC operator imaging solution, as in the standard TR formulation. Here, however, we emphasize the localization properties of the beam based data matrix and TR matrix.

This localization properties allow us to associate subrank matrices with appropriate sub-domains of the target domain, thus drastically reducing the number of data points involved in the computation.

2. Problem formulation and the beam based data matrix

A medium containing N_Q point scatterers (targets), located at $\mathbf{r}_q, \quad q = 1, ..., N_Q$, inside a domain V, is illuminated by discrete array of N^α collimated beam sources tagged by the index j. Each beam is also associated with the phase space index $\boldsymbol{\mu}_j^\alpha = (\mathbf{r}_j^\alpha, \boldsymbol{\xi}_j^\alpha)$ denoting, respectively, the beam initiation point and direction. We use iso-diffracting Gaussian beams (ID-GB) which are characterized by frequency independent collimation length [3], denoted here as b^α. The advantages of using ID-GB's are: (a) the beam propagation parameters through the ambient medium can be calculated only once and then used for all frequencies; (b) properly chosen ID-GB have been shown to provide efficient UWB frame expansion of arbitrary fields [10]; (c) because of these properties, the ID-GB can readily be transformed to the TD where they give rise to analytically trackable PB solutions [3]. Likewise, the receiver array consists of collimated receivers, tagged by the index i, and characterized appropriately by the similar parameters with superscript β replacing α. We mark the corresponding ID-GB solutions by $B_{\boldsymbol{\mu}_j^\alpha}(\mathbf{r})$ or $B_{\boldsymbol{\mu}_i^\beta}(\mathbf{r})$.

The beam based data matrix is the beam equivalent of the standard Green's function data matrix that appears in the classic TR literature [1, 2]. For point scatterers, neglecting multiple scattering, it may be expressed effectively by the outer product form

$$\mathbf{K} = \sum_{q=1}^{N_Q} M_q(\omega) \mathbf{b}_q^\beta \left(\mathbf{b}_q^\alpha\right)^t, \qquad \mathbf{b}_q^\alpha = [B_{\boldsymbol{\mu}_1^\alpha}(\mathbf{r}_q), ..., B_{\boldsymbol{\mu}_{N_\alpha}^\alpha}(\mathbf{r}_q)]^t, \quad \mathbf{b}_q^\beta = [B_{\boldsymbol{\mu}_1^\beta}(\mathbf{r}_q), ..., B_{\boldsymbol{\mu}_{N_\beta}^\beta}(\mathbf{r}_q)]^t \tag{1}$$

where $\mathbf{b}_q^\alpha$ and $\mathbf{b}_q^\beta$ are vectors of source and receiver beams calculated at the q target position $\mathbf{r}_q$ and the superscript t denotes the vector transposed. Here $M_q(\omega)$ denotes the frequency dependent strength of target q, and to simplify the formulation we also includes in this term the reciprocity factor relating the receiving and transmission pattern of the transducers. Note that due to the beam localization, all terms in the vectors (1) are negligibly small except those corresponding to beams passing near the q target (typically, for 1% error a three beamwidths neighborhood is sufficient), thus the qth matrix inside the data matrix $\mathbf{K}$ in (1) is sparse. For the readers convenience, the ij-element in $\mathbf{K}$ is written explicitly as

$$K_{ij} = \sum_{q=1}^{N_Q} M_q(\omega) B_{\boldsymbol{\mu}_i^\beta}(\mathbf{r}_q) B_{\boldsymbol{\mu}_j^\alpha}(\mathbf{r}_q), \tag{2}$$

and describes the measured i received beam scattered from the targets due to the j-th transmitted beam.

To illustrate the concepts of selective illumination, we consider the following example depicted in Fig. 1: choosing the wavelength to be 1, the sources and receivers arrays of 11 elements each are located at the $z = 0$ and $z = 200$ planes, symmetrically about $x = 0$ with inter-element distance $d = 5.1$. For simplicity, only two targets are considered, a weak target $M_1 = 1$ and a stronger one $M_2 = 100$ located at $(x, z) = (50, 100)$ and $(0, 100)$, respectively (right and left targets in Fig. 1). We are interested in imaging the sub-domain centered at $(x, z) = (60, 100)$, containing only the weaker target M_1 but not the stronger one M_2. The figure depicts also the axes of the beams, 79 beams from each array, covering the sub-domain of interest including its three beamwidths neighborhood. As discussed above, we use collimated ID-GB's with collimation length $b = 130$. The data matrix obtained for these beams is, in fact, a minor of the full data matrix obtained when the entire domain V is illuminate by beams. Figs. $2a$ and b depict the contribution to the data matrix $\mathbf{K}$ due to targets M_1 and M_2, respectively. Each square in these matrixes is associated with a pair of source and receiver points, while the inner structure inside the square is associated with pairs of source-receiver beams emerging from that point. Note that the contribution of target M_2 which is outside the sub-domain of interest is orders of magnitude weaker than that of M_1, even though its strength is much larger.

3. The beam based time reversal operator and its properties

We now define the beam-based $[N_\alpha \times N_\alpha]$ time-reversal operator $\mathbf{T}$ via

$$\mathbf{T} = \mathbf{K}^\dagger \mathbf{K} = \sum_q \sum_{q'} \Lambda_{q,q'} \left(\mathbf{b}_q^\alpha\right)^* \left(\mathbf{b}_{q'}^\alpha\right)^t \quad \text{where} \quad \Lambda_{q,q'} = M_q^* M_{q'} \left(\mathbf{b}_q^\beta\right)^\dagger \mathbf{b}_{q'}^\beta \tag{3}$$

(note that the expressions for $\mathbf{T}$ and $\Lambda_{q,q'}$ involve an outer and an inner vector products, respectively). Like the beam-based data matrix $\mathbf{K}$, $\mathbf{T}$ is also sparse, consisting of minors involving pairs of source and receiver beams that intersect near the targets. Its minors are therefore associated essentially with the sub-domains of the target domain V. Concentrating, for example, on a sub-domain of interest and considering the receivers beams $\boldsymbol{\mu}^{\beta}$ that pass within or near that sub-domain, one readily finds that the only non negligible elements of the matrix $\Lambda_{q,q'}$ are those located in that sub-domain. Furthermore, well resolved targets within this sub-domain (i.e., those separated by a wavelength or more) appear essentially on the diagonal of that minor, due to the phase cancelation in the summation (i.e., in the inner product of $\mathbf{b}_q^{\beta}$ in expression (3) for $\Lambda_{q,q'}$). Further localization of the minors of $\mathbf{T}$ is observed by considering the source beams $\boldsymbol{\mu}^{\alpha}$ that pass within that sub-domain. These localization properties imply that the image of a given sub-domains of V can be calculated by considering the corresponding low-rank minors of $\mathbf{T}$ instead of the full matrix $\mathbf{T}$ as in the conventional TR analysis. Note also that unlike conventional TR analysis, these minors are free of scattering data from other domains in V, which may otherwise dominate the data (as in the scenario considered in Fig. 1 where M_2 is much stronger than the target M_1 of interest, cf. Fig. 2).

Since for well resolved targets the matrix $\Lambda_{q,q'}$ is diagonal, one readily finds from (3) that $\left(\mathbf{b}_q^{\alpha}\right)^*$ form the set of eigenvectors of $\mathbf{T}$. In the *selective focusing* imaging scheme, these eigenvectors are used as initial amplitudes of the beam-source array, giving rise to the focusing field

$$u^q(\mathbf{r}) = \left(\mathbf{b}_q^{\alpha}\right)^{\dagger}\mathbf{b}^{\alpha}(\mathbf{r}), \qquad \text{where } \mathbf{b}^{\alpha}(\mathbf{r}) = [B_{\boldsymbol{\mu}_1^{\alpha}}(\mathbf{r}), ..., B_{\boldsymbol{\mu}_{N_{\alpha}}^{\alpha}}(\mathbf{r})]^t. \tag{4}$$

One may show that this field focuses at the qth target, hence it describes the point spread function (PSF) of this imaging algorithm. Fig. 3 shows the beams focused field (4), using the first eigenvector of $\mathbf{T}$ as the initiation amplitude of the beams. Notice the cross-axial resolution compared to the axial resolution, where the latter can be increased by using the temporal spectrum of the sources (either in the multi-frequency domain or in the short-pulse domain. Note that the focusing field in Fig. 3 corresponds here to the only non-singular eigenvalue of $\mathbf{T}$. Note also that the strong but non-desired target M_2 is not illuminated and therefore does not "contaminate" the data. Finally, the beam localized excitation also reduces the effect of multiple cross-targets scattering since targets outside the sub-domain of interest are weakly excited.

4. Concluding remarks

We presented a generalization of the classical Green's function TR imaging to a localized beam-based imaging via focusing. We considered the localization properties of the data matrix and the use of the minors of that matrix to form images of the corresponding sub-domain in the target domain. Other advantages are the relatively clean and low rank data, since targets in other sub-domains do not contribute to the data matrix corresponding to the sub domain of interest.

5. Acknowledgement

This work is supported in part by the Israeli Science Foundation, under Grant No. 674/07, and by NATO's Public Diplomacy Division in the framework of "Science for Peace" program, under Grant No. SfP982376.

6. References

1. C. Prada, J. L. Thomas, M. Fink, "The iterative time reversal process: Analysis of the convergence," *J. Acoust. Soc. Am.*, **97**, 1995, pp. 62–71.
2. A. J. Devaney, "Super-Resolution Processing of Multi-static Data Using Time Reversal and MUSIC," 2000. Unpublished manuscript available on the web site www.ece.neu.edu/faculty/devaney.
3. E. Heyman and L. B. Felsen, "Gaussian beam and pulsed beam dynamics: complex source and spectrum formulations within and beyond paraxial asymptotics," *J. Opt. Soc. Am. A*, **18**(7), 2001, pp. 1588–1610.
4. M. M. Popov, "A new method of computation of wave fields using Gaussian beams," *Wave Motion*, **4**, 1982, pp. 85–97.
5. V. Červený, "Gaussian beam synthetic seismogram," *J. Geophys.*, **58**, 1985, pp. 44–72. 1985.
6. G. F. Edelmann, J. F. Lingevitch, C. F. Gaumond, D. M. Fromm, D. C. Calvo, "Comparison of a subrank to a full-rank time reversal operator in a dynmaic ocean," *J. Acoust. Soc. Am.*, **122**, 2007, pp. 2706–2714.

7. T. Melamed, E. Heyman, and L. B. Felsen, "Local spectral analysis of short-pulse-excited scattering from weakly inhomogeneous media. Part I: Forward scattering," *IEEE Trans. Antennas Propagat.*, **47**, 1999, pp. 1208–1217.
8. B. Rao, L. Carin, "Beam-tracing-based inverse scattering for general aperture antennas," *J. Opt. Soc. Am. A*, **16**, 1999, pp. 2219–2231.
9. N. R. Hill, "Prestack gaussian-beam depth migration," *Geophysics*, **66**(4), 2001, pp. 1240–1250.
10. A. Shlivinski, E. Heyman, A. Boag, and C. Letrou, "A phase-space beam summation formulation for ultra wideband radiation," *IEEE Trans. Antennas Propagat.*, **52**, 2004, pp. 2042–2056.

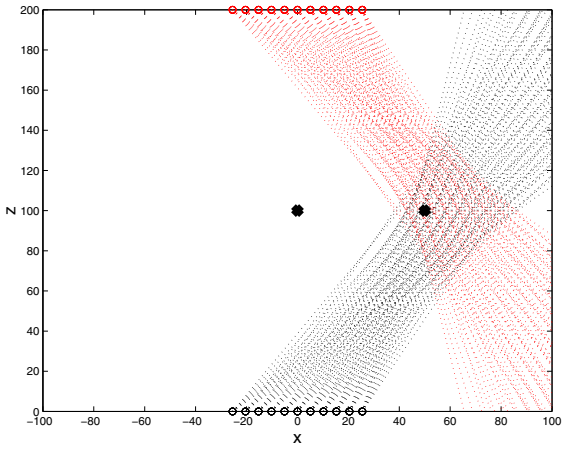

Figure 1: Physical configuration. A weak target $M_1 = 1$ and a stronger one $M_2 = 100$ located at $(x, z) = (50, 100)$ and $(0, 100)$, respectively. The beam axes emerging from the source and receiver arrays, are chosen to cover only the sub-domain of interest.

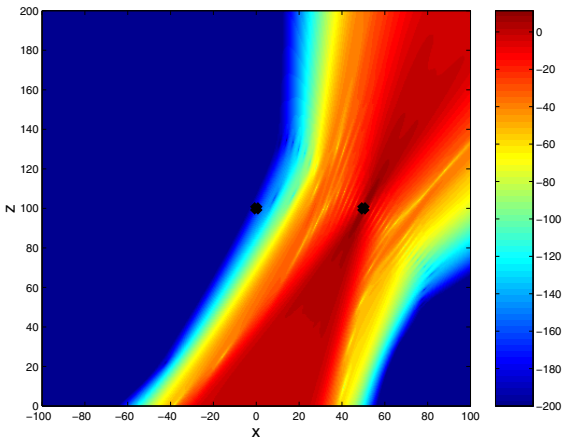

Figure 3: The focusing field (4) for target M_1

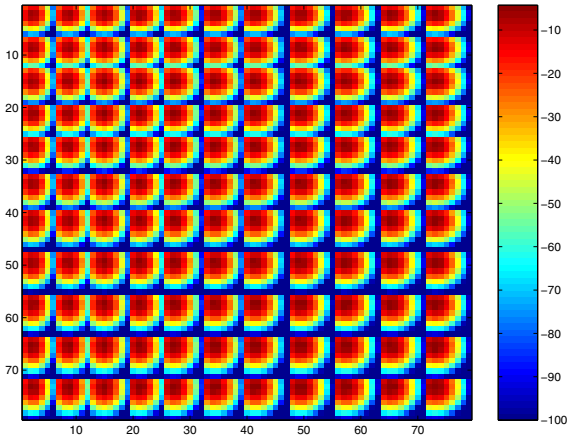

Figure 2a: The contribution of target M_1 to the data matrix $\mathbf{K}$. The squares are associated with pairs of source and receiver points, while the inner structure inside the squares is associated with pairs of source-receiver beams emerging from these points.

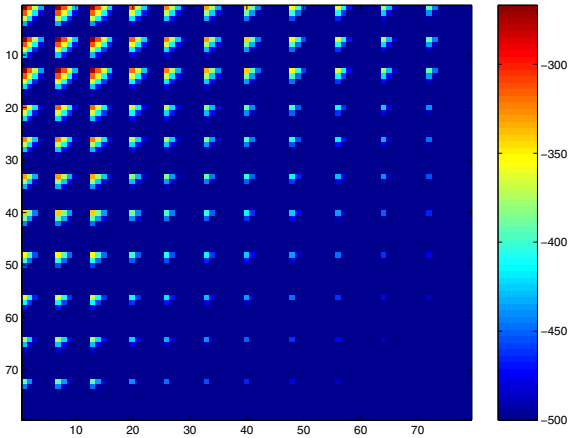

Figure 2b: As in Figure 2a but for the non-illuminated, yet stronger target M_2. This contributions is orders of magnitude weaker than that of M_1 (note the difference in scales of these figures).